Journal of Power Sources 195 (2010) 5868–5874

Contents lists available at ScienceDirect

Journal of Power Sources

journal homepage: www.elsevier.com/locate/jpowsour

Synthesis and properties of samaria-doped ceria electrolyte for IT-SOFCs by EDTA-citrate complexing method

Wen-Chang Wu[a,*], Jui-Ting Huang[a], Atsushi Chiba[b]

[a] Department of Chemical and Material Engineering, Southern Taiwan University, 1 Nan-Tai St., Yung-Kung City, Tainan 710, Taiwan
[b] Department of Materials Chemistry, Faculty of Engineering, Yokohama National University, 79-5, Tokiwadai, Hodogaya-ku, Yokohama, Japan

ARTICLE INFO

Article history:
Received 21 October 2009
Received in revised form
13 December 2009
Accepted 28 December 2009
Available online 13 January 2010

Keywords:
Samaria-doped ceria (SDC)
Intermediate-temperature solid oxide fuel cells (IT-SOFCs)
EDTA-citric complexing method
Organic compound
Electrical conductivity

ABSTRACT

An ultra-fine samaria-doped ceria ($Ce_{0.8}Sm_{0.2}O_{1.9}$, SDC) electrolyte prepared by a non-ion selective EDTA-citric complexing method is developed herein for intermediate-temperature solid oxide fuel cells (IT-SOFCs). The rigid agglomerates due to organic compounds that exist in the SDC precursors during the EDTA-citrate complexing synthesis process inhibit crystalline growth and grain growth, leading to the generation of ultra-fine grain following the sintering procedure. Calcination is necessary above 500 °C for all precursors. The average grain size of the pellets after sintering at 1400 °C for 2 h is submicron in scale (from 200 nm to 600 nm) with various pH values, and the pellets are smaller than those obtained from other synthesis processes. Dense pellets with pH values of 10 (relative density of 99%) are obtained with precursor powder calcination at 900 °C for 3 h. Electrical conductivity is dependent on the calcination temperature and pH value of the solution, and the maximum electrical conductivity is 0.01 S cm^{-1} at 700 °C with a pH value of 10.

1. Introduction

Solid oxide fuel cells (SOFCs) have the potential of being the cleanest, most efficient and most versatile technology for chemical-to-electrical energy conversion. SOFC technology has demonstrated high energy efficiency with minimal pollutant emission, as compared to conventional energy technology; however, the cost of the current SOFC systems is prohibitive for wide commercial applications [1]. To be economically competitive, the cost of materials and fabrication must be dramatically reduced. One effective approach for achieving cost reduction is to reduce the operating temperature so that interconnections, heat exchanges and structural components can be fabricated from relatively inexpensive metals. Some ways the operating temperature can be reduced include the improving electrode microstructure or increasing the component uniformity of the electrolyte, using an electrolyte of high ionic conductivity at low temperatures, as well as by reducing electrode-to-electrolyte interfacial resistance [2,3].

Yttria-stabilized zirconia (YSZ), the electrolyte for SOFC, has been regarded as a most promising material due to its high conductivity and its transference number of oxide ions with a higher operative temperature; however, its operating temperature must be 1000 °C [4]. Recently, the systematic ceramic powders of rare-earth elements-doped ceria have been investigated as a new type of electrolyte material which can reduce the operating temperature of SOFCs [5,6]. Doped ceria actually has an ionic conductivity higher than that of YSZ at all temperatures below 800 °C [7]. However, many researchers have been reported that a reduction of Ce^{4+} to Ce^{3+} by hydrogen occurs at the anode side above 450 °C, causing low open-circuit voltage (OCV) and thus energy loss [7,8]. There are several ways can avoid or reduce these losses, such as form a barrier layer between the anode and electrolyte like BaO [8] or YSZ [9]. The oxygen-ion conductivities of ceria-based electrolytes doped with various ions at different concentrations have been extensively studied [10–13]. Among them, Sm^{3+}-doped CeO_2 was found to exhibit the highest oxygen-ion conductivity at certain fixed doping levels because it had the smallest association enthalpy between the dopant cations and the oxygen vacancies in the fluorite lattice [14,15]. Actually, many researchers have demonstrated high performance SOFCs using samaria-doped ceria (SDC) as the electrolyte at low temperatures [16–18].

Electrolyte conductivity is mainly affected by the grain boundary and grain resistance which are, in turn, affected by the grain size. The influence of grain size on the conductivity of highly doped ceria in the submicron/micron [19,20] and the nano-grain size [21,22] range has been studied.

Many methods have been developed that can lead to nanocrystalline powder [23]. The pyrolysis of complex gel has been used extensively in the synthesis of functional oxides. This method is known as the Pechini method [24], and it has the advantage of not

* Corresponding author. Tel.: +886 6 2533131 6947; fax: +886 6 2425741.
E-mail address: wchang@mail.stut.edu.tw (W.-C. Wu).

0378-7753/$ – see front matter © 2010 Elsevier B.V. All rights reserved.
doi:10.1016/j.jpowsour.2009.12.098

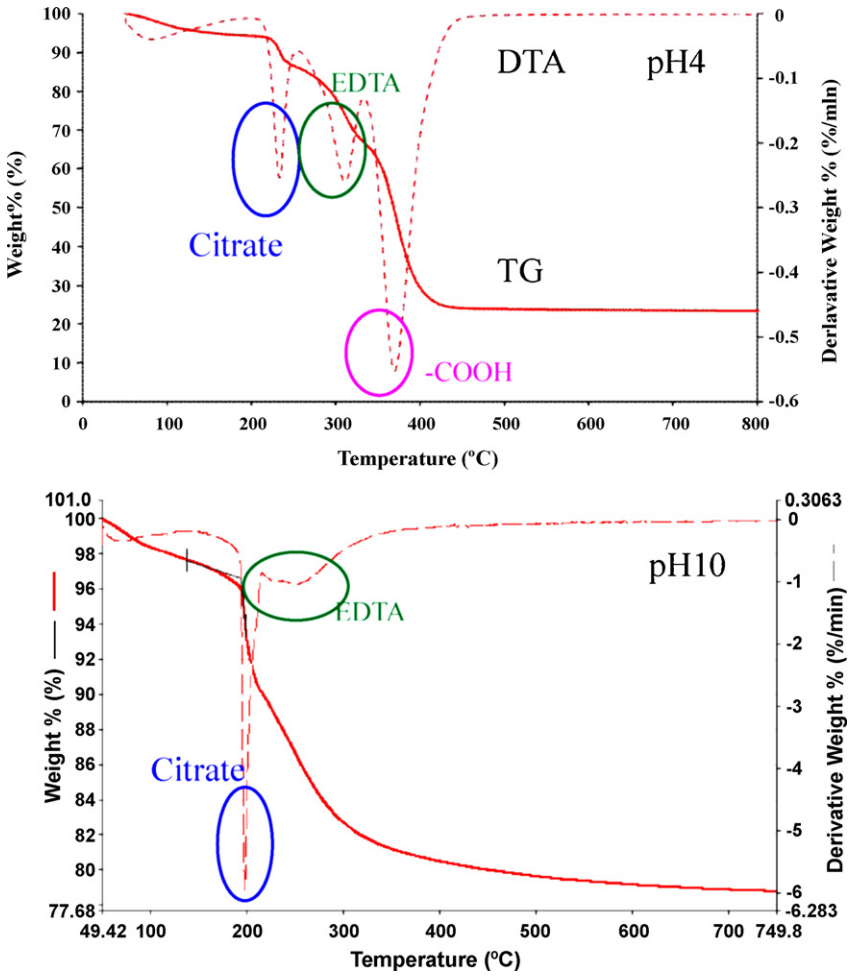

Fig. 1. TG-DTA curve of precursor powders pre-dried to a soft gel at 80 °C with a pH of 10.

requiring the formation of suitable hydroxo complexes for the metals involved. Chelating agents tend to form stable complexes with a variety of metals over fairly wide pH ranges, thus allowing for a relatively easy synthesis of oxides of considerable complexity. The success of a combined complexing process with triethanolamine (EDTA) and sucrose as the complexing agents in the synthesis of nanocrystalline $La_{0.6}Sr_{0.4}Co_{0.2}Fe_{0.8}O_{3-\delta}$ (LSCF) [25], YSZ [25], $Ba_{1-x}Sr_xTiO_3$ [26] and ScSZ [27] has been recently reported.

In the present study, an ultra-fine samaria-doped ceria ($Ce_{0.8}Sm_{0.2}O_{1.9}$, SDC) electrolyte prepared by the EDTA-citric complexing method was developed for intermediate-temperature solid oxide fuel cells (IT-SOFCs). The influence of pH value on the synthesis of SDC powder based on the combined EDTA–citrate complexing process has been investigated. The influence of calcination temperature and pH value on grain resistance and grain boundary resistance due to grain size after sintering was also investigated in this study.

2. Experiment

2.1. Preparation of SDC electrolyte

All the chemical reagents used in this experiment were of analytical grade. Typically, metal nitrates and oxides were used as the metal sources. Stoichiometric amounts of 0.08 M $(NH_4)_2Ce(NO_3)_6$ and 0.02 M Sm_2O_3 were pre-dissolved in deionized water and then mixed into an aqueous solution at room temperature. The necessary amount of EDTA dissolved in an NH_3 solution was then dropped into the mixed metal nitrate solution, followed by the addition by stirring of solid citric acid (mole ratio of total metal ions to EDTA and to citrate = 1:1:2). Then, NH_4OH was used to adjust the pH of the solution to the desired value. The solution was heated, and above 80 °C it turned into a transparent gel; it was then heated in a 180 °C oven to convert it to a solid precursor. Next, the precursor was calcined at a high temperature in air for the preparation of a dense ceramic electrolyte. The synthesized powders were uniaxially pressed into green discs (13 mm in diameter) under the pressure of 300 MPa, followed by sintering at 1400 °C for 2 h in air, for densification of the electrolyte.

2.2. Characterization

Thermogravimetric analysis (TGA) of the powders was performed using a Netzsch STA449C simultaneous thermal analyzer at a heating rate of 10 °C min^{-1} in air. The microstructures of the SDC powders were characterized using X-ray powder diffraction (XRD) and following the rule of Ni-filtered CuKα radiation (Rigaku MultiFlex, Japan). The morphology of the SDC powders was analyzed using a scanning electron microscope (SEM, Hitachi S-3000N, Japan) and a transmission electron microscope (TEM, Philips Tecnai G2 F20 FEG-TEM, Netherlands). The average crystalline size of the powder was calculated by adopting the XRD data and the Scherrer formula as follows [28]:

$$D = \frac{0.9\lambda}{\beta \cos \theta} \quad (1)$$

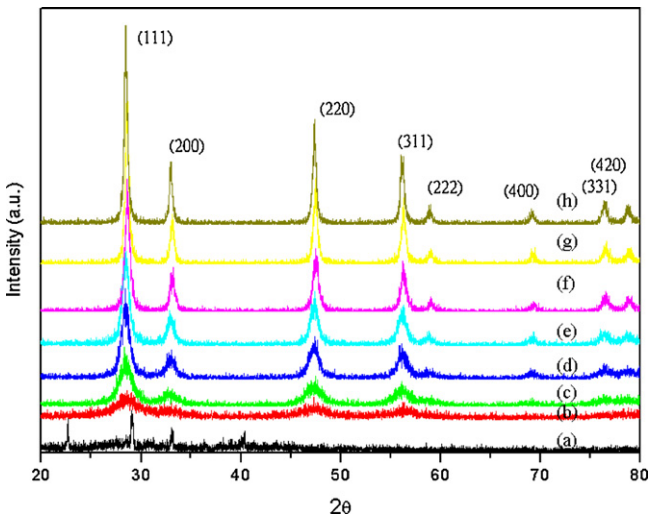

Fig. 2. XRD patterns of gel and calcined samples at various calcination temperatures for 3 h with a pH value of 10: (a) precursor powder; (b) 300 °C; (c) 400 °C; (d) 500 °C; (e) 600 °C; (f) 700 °C; (g) 800 °C; and (g) 900 °C.

where D is the crystalline size, λ the wavelength of the incident X-rays (CuKα; $\lambda = 0.15406$ nm), θ the diffraction angle, and β the corrected half-width. Relative density was determined by the Archimedes method. The composition of the SDC powder was analyzed using an energy dispersive spectrometer (Philips Tecnai G2 F20 FEG-TEM). The ionic conductivity of the SDC electrolytes was determined by an electrochemical workstation (Hioki 3532-50 LCR Hitester, Japan) at an operation temperature ranging from 500 °C to 700 °C.

3. Results and discussion

3.1. Characterization of SDC precursor powders

$Ce_{0.8}Sm_{0.2}O_{1.9}$ (SDC) powders prepared by a non-ion selective EDTA-citric complexing method for intermediate-temperature solid oxide fuel cells (IT-SOFCs) were first investigated. After the evaporation of water at 80 °C, the deep yellow gel of the EDTA complex was obtained. The gel was pre-dried to a soft gel at 80 °C, and the solid precursor dried at 180 °C for 18 h in air. Thermal analysis of the soft gel was performed after the pre-drying at 80 °C. Fig. 1 shows the TG-DTA curves of the precursor powders that were prepared in solution with a pH value of 4 and 10. The corresponding DTA curves had two same endothermic peaks with pH values of 4 and 10: one at 200 °C for the citrate and the other at 260 °C for the EDTA complex formation, however, the third endothermic peak was only observed at 370 °C for carboxyl group with a pH value of 4. In addition, the weight loss increased with decreasing pH values, from 20% with a pH of 10 to 78% with a pH of 4 in the temperature range of 300–500 °C, respectively. It was indicated that many organic compounds (e.g., citrate and EDTA complex) existed in the SDC precursors during the EDTA-citrate complexing synthesis process, especially in the acidic condition, because the chelating specimens of EDTA and critic acid decomposition were H_2Y^{2-} and H_2L^-, and had a large amount of carboxyl groups existed in these complexes with a pH value of 4. These organic compounds existed in the precursors were likely to affect the sintering characteristics; therefore, the precursors were calcined above 500 °C before sintering. The precursor was calcined at various temperatures for 3 h in air. Fig. 2 shows the corresponding XRD patterns of the gel and the calcined samples. It was found that the initial dry gel exhibited a metal-citrate and a metal-EDTA phase with no appearance of an SDC crystallization phase. However, a significant single phase cubic fluorite structure formed when the calcination temperature was 400 °C or higher.

The relative densities of the SDC pellets, with calcination temperatures ranging from 600 °C to 900 °C and after sintering at 1400 °C for 2 h in air, are indicated in Fig. 3. The pellets that were calcined at 600 °C, 700 °C, 800 °C, and 900 °C all had a density of over 95%. It was indicated that the organic compounds could be eliminated completely at calcination temperatures of 600 °C to 900 °C. Furthermore, a higher calcination temperature resulted in a denser

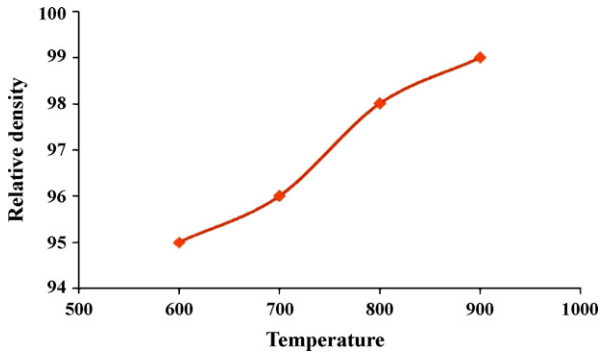

Fig. 3. Relative densities of SDC pellets with calcination temperatures from 600 °C to 900 °C and sintered at 1400 °C for 2 h in air with a pH value of 10.

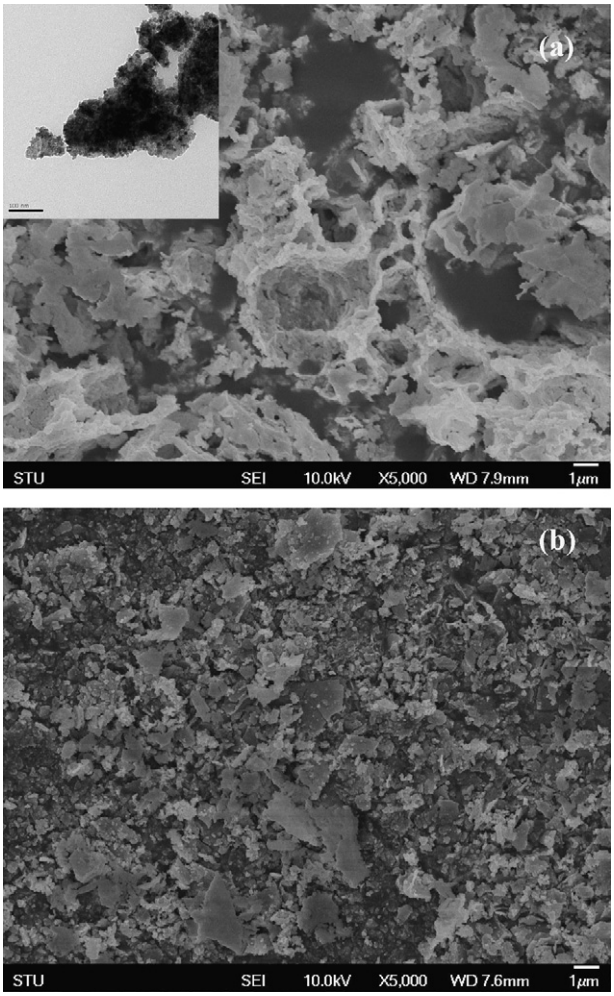

Fig. 4. SEM micrographs of SDC powders calcined at (a) 600 °C (small window: TEM image) and (b) 900 °C for 3 h with a pH value of 10.

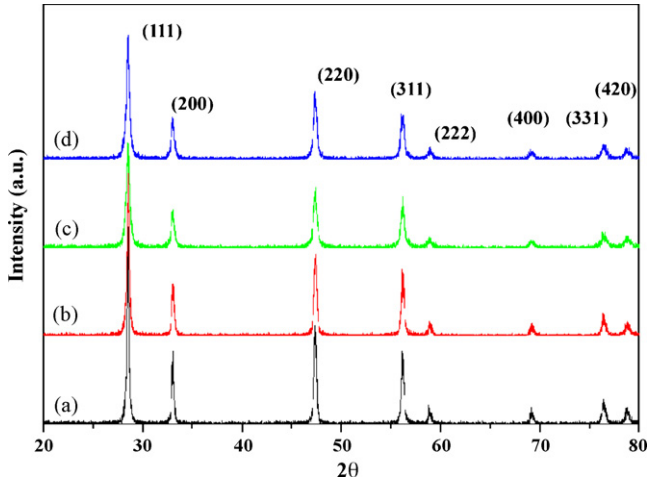

Fig. 5. XRD patterns of SDC powders with various pH values after calcination at 900 °C: (a) 4; (b) 6; (c) 8; (d) 10.

structure, e.g., a relative density of 99% with calcination at 900 °C. However, the morphologies of the SDC powders after calcination at different temperatures were significantly different, as shown in Fig. 4. The SEM image of the morphology of the sample powders after calcination at 600 °C exhibited a more reticular structure, e.g., an rigid agglomerate shape of the resulting oxides, but these agglomerative reticular structure collapsed completely into a particle/sheet structure after calcination at 900 °C. It was indicated that the rigid agglomerate structure was formed due to the organic compounds existed in precursors after calcination at low temperature (small window in Fig. 4(a)), and that it resulted in lower densities.

3.2. Effects of pH value on SDC synthesis and properties

Fig. 5 depicts the XRD patterns of the SDC powders with pH values ranging from 4 to 10 after calcination at 900 °C. The single phase fluorite structure obtained a full range of pH values. The crystalline size (D) of the samples was determined from the X-ray line broadening using Scherrer's equation (Eq. (1)). The average cystalline size of the SDC powder decreased from 30 nm to 20 nm with increasing pH values (Fig. 6). It was obvious that SDC crystalline growth after calcination with low pH values was faster than that with high pH values because the formed crystal was smaller when synthesized under acidic conditions [29].

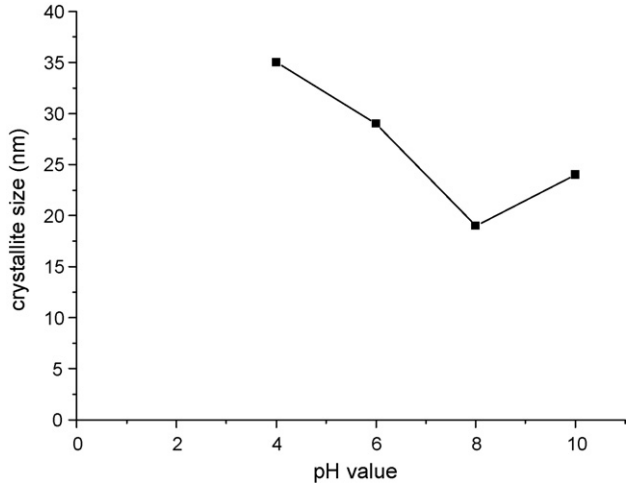

Fig. 6. Average crystalline size of SDC powders with various pH values after calcination at 900 °C.

Table 1
Compositions of SDC powders after calcination at 900 °C for 3 h with various pH values in solution.

Composition (atom%)	pH value			
	4	6	8	10
Ce	78.7	80.3	80.5	79.6
Sm	21.4	19.7	19.5	20.4

An energy dispersive spectrometer (EDS) was used to compare the compositional variations of product powders with various pH values. Table 1 indicates the composition of the SDC powders after calcination at 900 °C with various pH values. The Ce/Sm composition ratio of the SDC powders for all the samples was 8:2, which was close to the stoichiometric composition of the starting materials, and the ratio remained almost unchanged with various pH values. This result differed significantly from that of the Pechini method based on citric acid as the complexing agent [26] or on EDTA as the chelating agent [27]. The equilibrium concentration of various species of EDTA (H_4Y, H_3Y^-, $H_2Y_2^-$, HY^{3-} and Y^{4-}) and citrate (H_3L, H_2L^-, HL^{2-} and L^{3-}) was pH dependent (Fig. 7) [25]. The major formation equations of stable metal–EDTA and metal–citrate complexes in acidic and alkali sides were [20]:

$$Ce^{4+} + H_2L^- = Ce(H_2L)^{3+}, \quad (pH < 6) \tag{2}$$

$$Ce^{4+} + HL^{2-} = Ce(HL)^{2+}, \quad (pH < 6) \tag{3}$$

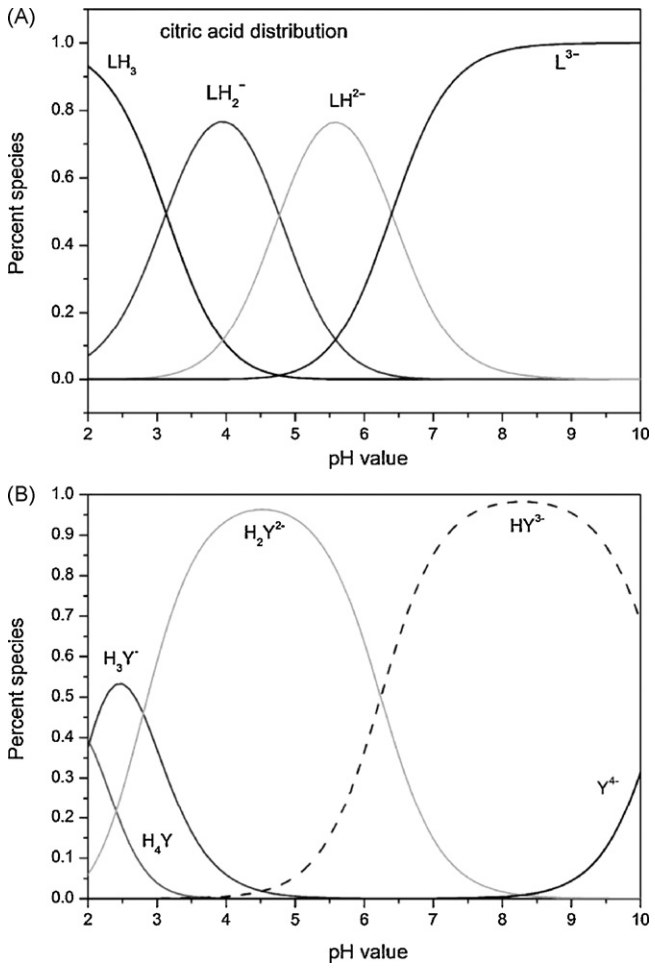

Fig. 7. pH dependence of the equilibrium distribution of various species of EDTA (H_4Y, H_3Y^-, $H_2Y_2^-$, HY_3^- and Y_4^-) (B) and citrate (H_3L, H_2L^-, HL_2^- and L_3^-) (A). [20].

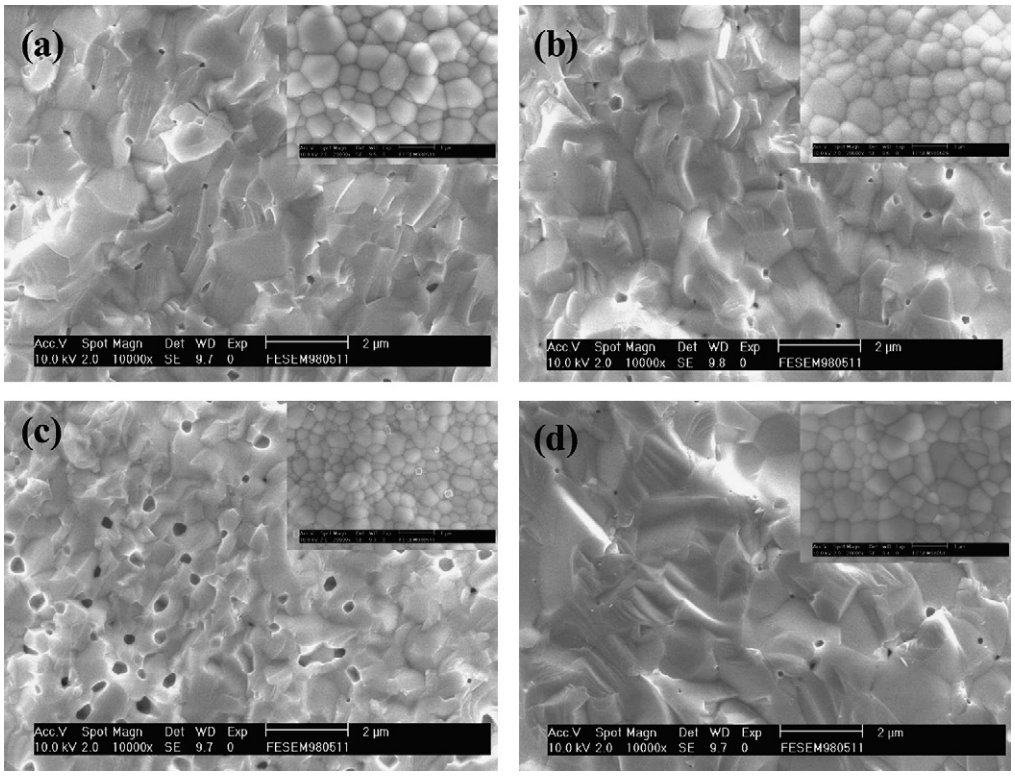

Fig. 8. Top-view (small window) and cross-sectional SEM images of pellets sintered at 1400 °C in air under different pH values: (a) 4; (b) 6; (c) 8; (d) 10.

$$Sm^{3+} + H_2L^- = Sm(HL)^{2+}, \quad (pH < 6) \tag{4}$$

$$Sm^{3+} + HL^{2-} = Sm(HL)^{+}, \quad (pH < 6) \tag{5}$$

$$Ce^{4+} + HY^{3-} = Ce(Y)^{+}, \quad (pH > 8) \tag{6}$$

$$Ce^{4+} + Y^{4-} = Ce(Y), \quad (pH > 8) \tag{7}$$

$$Sm^{3+} + HY^{3-} = Sm(Y), \quad (pH > 8) \tag{8}$$

$$Sm^{3+} + Y^{4-} = Sm(Y)^{-}, \quad (pH > 8) \tag{9}$$

Moreover, the remaining good properties of the powders obtained at a low pH (pH < 5) by the EDTA–citrate process demonstrated the effectiveness of citrate as a second complex agent to preserve the homogeneity of the mixing in the process. The existence of a stable complex of metal ions with partially deprotonated citrate helped preserve the homogeneity of the EDTA–citrate–metal precursor at low pH values [25]. Therefore, a uniform composition in the wide range of pH values was obtained by the EDTA–citrate complexing method.

Top-view (small window) and cross-sectional SEM images of the pellets sintered at 1400 °C in air under different pH values are shown in Fig. 8. All electrolytes exhibited dense sintered bodies under various pH values, as indicated in the top-view SEM images. However, the pellets formed many pores at a pH value of 8, as depicted in the cross-section micrographs. The same results were obtained in the investigation of the relative density of sintered bodies by the Archimedes method (Fig. 9). It was found that the SDC pellets, with powder derived from the EDTA–citrate–metal precursor calcined at 900 °C for 3 h, displayed a sintering density of >95% with a pH of 8 after sintering at 1400 °C for 2 h, and nearly 99% with a pH value of 10. The morphology of the SDC powders still exhibited an agglomerative reticular structure after calcination at 900 °C with a pH value of 8, compared with those obtained at other pH values and caused to has a poor sinterability has been observed in the investigated of SEM images of powders after calcination. The average grain size from these images has been summarized in Table 2.

It was found that the average grain size of the pellets was nearly nano-scale and depended on pH values. The average grain size was 477–494 nm for pH values of 4 and 10, 522 nm for a pH of 6, and 366 nm for a pH of 8, respectively. The results indicated that the average grain with a pH of 8 was smaller than that with other pH values; however, the crystalline size of the SDC powders after calcination was smaller with a pH of 8 than that obtained with other pH values, as depicted in Fig. 6. Usually, a small crystal with a high surface-activity can grow a larger grain during the sintering process. However, the opposite results were found in this work. The comparatively small sintered grain size of the pH 8 powder is surprising since the calcined pH 8 powders had the smallest initial grain size. Since both particle size and morphology can influence grain growth, this behavior is probably due to the large amount of rigid agglomerative reticular structure which existed in the calcined SDC powders made with a pH 8.

Typical impedance spectra for SDC electrolytes were shown in Fig. 10. The spectra for all samples with various pH values were well separated into two semicircles. The contribution of the grain

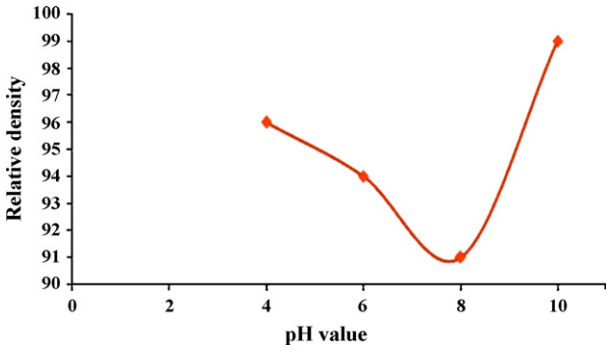

Fig. 9. Relative densities of SDC pellets with various pH values after sintering at 1400 °C for 2 h in air.

Table 2
Relationships of average grain size and electrical conductivity of SDC pellets after sintering at 1400 °C for 2 h in air with various pH values in solution.

pH value	Measure temperature (°C)	Average grain size (nm)	Grain boundary width (nm)	Bulk conductivity σ_b (S cm^{-1})	Specific grain boundary conductivity σ_{gb} (S cm^{-1})[a]	Total conductivity σ (S cm^{-1})	Activity energy (kJ mol^{-1})
4	700	494	15	1.2×10^{-1}	1.9×10^{-4}	6.1×10^{-3}	74
	600			7.2×10^{-2}	6.4×10^{-6}	2.1×10^{-3}	
	500			2.9×10^{-2}	1.8×10^{-6}	5.9×10^{-4}	
6	700	522	15	1.5×10^{-1}	1.3×10^{-4}	4.4×10^{-3}	71
	600			7.9×10^{-2}	5.5×10^{-6}	1.9×10^{-3}	
	500			3.0×10^{-2}	6.4×10^{-6}	5.2×10^{-4}	
8	700	366	15	1.2×10^{-1}	1.1×10^{-4}	3.5×10^{-3}	70
	600			7.1×10^{-2}	6.2×10^{-6}	1.4×10^{-3}	
	500			2.8×10^{-2}	2.0×10^{-6}	4.8×10^{-4}	
10	700	477	15	1.1×10^{-1}	3.5×10^{-4}	1.0×10^{-2}	78
	600			6.5×10^{-2}	8.5×10^{-5}	2.6×10^{-3}	
	500			2.6×10^{-2}	2.2×10^{-5}	6.9×10^{-4}	

[a] Specific gb conductivity = measured gb conductivity × (gb width/grain size).

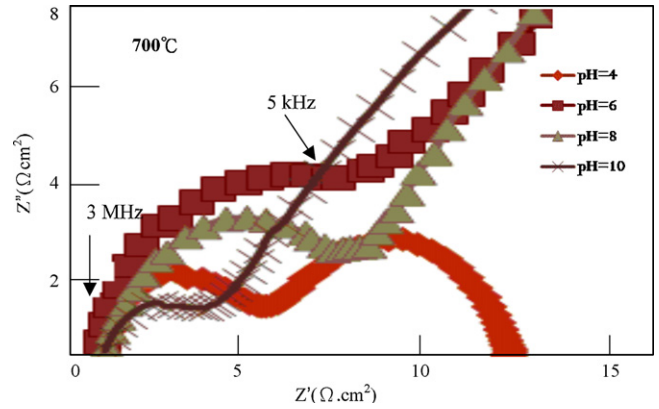

Fig. 10. Impedance spectra of SDC pellets sintered at 1400 °C for 2 h in air with various pH values in solution.

boundary resistance (high frequency part) and electrode resistance (low frequency part) were determined. It was found that the grain boundary resistance significantly depended on the pH values in solution. Fig. 11 indicates the total electrical conductivities, at temperatures ranging from 500 °C to 700 °C, of the SDC pellets sintered at 1400 °C for 2 h in air with various pH values in solution. The Arrhenius relationship can be expressed as $\sigma = (\sigma_0/T)\exp(-E_a/kT)$, where σ_0 is the pre-exponential factor, E_a the activation energy, and k the Boltzmann constant. Furthermore, $\ln(\sigma T)$ is plotted against $1000/T$, and a linear relationship should exist. Results indicated that the electrical conductivity of the SDC

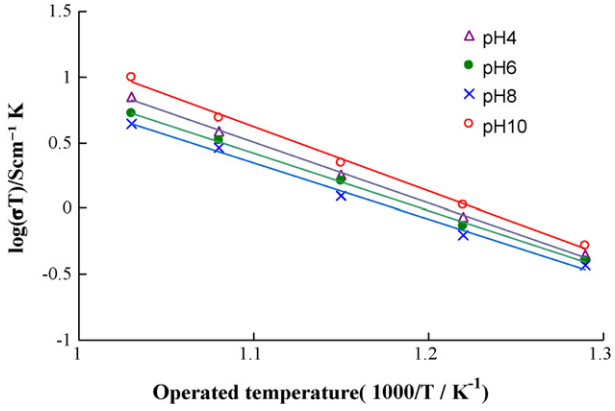

Fig. 11. Electrical conductivities in the temperature range of 500–700 °C of SDC pellets sintered at 1400 °C for 2 h in air with various pH values in solution.

pellets decreased with increasing pH values, from 6.1×10^{-3} S cm^{-1} with a pH of 4 to 3.5×10^{-3} S cm^{-1} with a pH of 8, then increased sharply to 1.0×10^{-2} S cm^{-1} at 700 °C when the pH value was 10. The results indicated that differences in the EDTA-citrate complexing in the solution influenced the particle/agglomerate shape of the resulting oxides with various pH values and calcinations temperature, and that these sometimes low density/rigid agglomerates resulted in lower densities, lower grain size, and lower total conductivity.

The electrical conductivity of the SDC electrolyte mainly depended on the resistances of bulk (grain, R_b) and grain boundary (R_{gb}). The value of R_b was determined from the total resistance (R_t) - R_{gb}, and that of R_{gb} was determined from the grain boundary arc according to the impedance diagram (Fig. 10); then they were converted to bulk (σ_b) and specific grain boundary (σ_{gb}) conductivities using equation (Eq. (10)), as shown in Table 2.

$$\text{Specific gb conductivity} = \text{measured gb conductivity} \times \left(\frac{\text{gb width}}{\text{grain size}}\right) \quad (10)$$

It was obvious that the specific grain boundary conductivity was smaller than the bulk conductivity for all samples synthesized with various pH values; however, the total electrical conductivity of the SDC electrolyte depended greatly on the synthesized condition of the pH value in solution. Of these samples the best electrical conductivity was 0.01 S cm^{-1} at 700 °C with a pH value of 10. A small grain size increased the grain boundary resistance of the pellet, but no significant difference existed in grain (bulk) conductivity. Similarly, Rambabu et al. reported that σ_{bulk} was less dependent on grain size, while σ_{bound} was greatly dependent on grain size [30]. A small grain size generated a high percentage of grain boundary region, hence, greater grain boundary resistance (see in Table 2). Furthermore, pores or defects in the grain boundary also increased resistance, because the lower connectivity formed due to the pores or defects resulted in low effective conductivity had been illustrated by effective media theories [31]. In addition, the values of activation energy were from 70 kJ mol^{-1} to78 kJ mol^{-1} with various pH values, and less or approach to the values in the literature. It was obvious that the SDC electrolyte synthesized with EDTA-citrate complexing route will be suitable to low temperature operation for SOFC.

4. Conclusions

The rigid agglomerates due to organic compounds that existed in the SDC precursors during the EDTA-citrate complexing synthesis process inhibited crystalline growth and grain growth, leading to the generation of ultra-fine grain electrolyte. Calcination above 500 °C was necessary for all precursors in this study. SDC powder

of a stable and uniform composition was prepared by the EDTA-citrate complexing method. The average crystalline size of the SDC powders was ≦30 nm after calcination at 900 °C for 3 h. The grain size of the pellets after sintering at 1400 °C for 2 h was submicron in scale, from 200 nm to 600 nm, with various pH values, and smaller than those prepared by other synthesis routes. The most dense pellets were obtained with a pH value of 10 (relative density of 99%), due to the precursor powders calcined at 900 °C for 3 h. The electrical conductivities were dependent on the calcination temperature and the pH value in solution, and the best electrical conductivity was 0.01 S cm^{-1} at 700 °C with a pH of 10. This study was successful in the preparation of different submicron grain-size SDC electrolytes by adjusting calcination temperature and pH value via the EDTA-citrate complexing method.

Acknowledgement

The financial support of this work by the National Science Council of the Republic of China, under contract NSC 97-2221-E-218-031-, is gratefully acknowledged.

References

[1] Masayuki Dokiya, Solid State Ionics 152–153 (2002) 383.
[2] C. Xia, M. Liu, Solid State Ionics 144 (2001) 249.
[3] Xi Chu, Won il Chung, L.D. Schmidt, J. Am. Ceram. Soc. 76 (8) (1993) 2115.
[4] K. Eguchi, N. Akasaka, H. Mitsuyasu, Y. Nonaka, Solid State Ionics 135 (2000) 589.
[5] K. Zheng, B.C.H. Steele, M. Sahibzada, I.S. Metcalfe, Solid State Ionics 86–68 (1996) 1241.
[6] B.C.H. Steele, Solid State Ionics 129 (2000) 95.
[7] K. Eguchi, T. Setoguchi, T. Inoue, H. Arai, Solid State Ionics 52 (1992) 165.
[8] Daisuke Hirabayashi, Atsuko Tomita, Shinaya Teranishi, Takashi Hibino, Mitsuru Sano, Solid State Ionics 176 (2005) 881.
[9] Tsai Tsepin, Perry Erica, Barnett Scott, J. Electrochem. Soc. 144 (1997) L130.
[10] D.Y. Wang, D.S. Park, J. Griffith, A.S. Nowick, Solid State Ionics 2 (1981) 95.
[11] G.B. Balazs, R.S. Glass, Solid State Ionics 76 (1995) 155.
[12] C. Tian, S.W. Chan, Solid State Ionics 134 (2000) 89.
[13] T.S. Zhang, P. Hing, H.T. Huang, J.A. Kilner, Solid State Ionics 148 (2002) 567.
[14] R. Gerhard-Anderson, A.S. Nowick, Solid State Ionics 5 (1981) 547.
[15] J.A. Kilner, Solid State Ionics 8 (1983) 201.
[16] Takashi Hibino, Atsuko Hashimoto, Takao Inoue, Jun-ichi Tokuno, Shin-ichiro Yoshida, Mitsuru Sano, Science 288 (2000) 2031.
[17] Zongping Shao, M. Sossina, Haile, Nature 431 (2004) 170.
[18] Takashi Hibino, Atsuko Hashimoto, Masaya Yano, Masanori Suzuki, Shin-ichiro Yoshida, Mitsuru Sano, J. Electrochem. Soc. 149 (2002) A133.
[19] C. Tian, S.-W. Chan, Solid State Ionics 134 (2000) 89.
[20] A. Tschope, S. Kilassonia, R. Birringer, Solid State Ionics 173 (2004) 57.
[21] Y.M. Chiang, E.B. Lavik, D.A. Blom, Nanostruct. Mater. 9 (1997) 633.
[22] T. Suzuki, I. Kosacki, H.U. Anderson, Solid State Ionics 151 (2002) 111.
[23] B.L. Cushing, V.L. Kolesnichenko, C.J. O'Connor, Chem. Rev. 104 (2004) 3893.
[24] M.P. Pechini, US Patent, 3 (1967) 330.
[25] Wei Zhou, Zongping Shao, Wanqin Jin, J. Alloys Compd. 426 (2006) 368.
[26] R.N. Das, P. Pramanik, Nanotechnology 15 (2004) 279.
[27] Hongxia Gu, Ran Ran, Wei Zhou, Zongping Shao, J. Power Sources 172 (2007) 704.
[28] Zhang Tianshu, Peter Hing, J. Haitao Huang, Kilner, Solid State Ionics 148 (2002) 569.
[29] Jyung-Dong Lin, Jenq-Gong Duha, Bi-Shiou Chiou, Mater. Chem. Phys. 68 (2001) 42.
[30] B. Rambabu, Samrat Ghosh, Weichang Zhao, Hrudananda Jena, J. Power Sources 159 (2008) 21.
[31] S. David, Mclachlan, Michael Blaszkiewicz, E. Robert, Newnham, J. Am. Ceram. Soc. 73 (8) (1990) 2187.